

Identification of symmetry-protected topological states on noisy quantum computers

Daniel Azses,^{1,2} Rafael Haenel,^{3,4} Yehuda Naveh,⁵ Robert Raussendorf,^{3,4} Eran Sela,⁶ and Emanuele G. Dalla Torre^{1,2}

¹*Department of Physics, Bar-Ilan University, Ramat Gan 5290002, Israel*

²*Center for Quantum Entanglement Science and Technology,
Bar-Ilan University, Ramat Gan 5290002, Israel*

³*Department of Physics and Astronomy,
University of British Columbia, Vancouver, BC V6T 1Z1, Canada*

⁴*Stewart Blusson Quantum Matter Institute,
University of British Columbia, Vancouver, BC V6T 1Z4, Canada*

⁵*IBM Research - Haifa, Haifa University Campus,
Mount Carmel, Haifa 31905, Israel*

⁶*School of Physics and Astronomy,
Tel Aviv University, Tel Aviv 6997801, Israel*

Abstract

Identifying topological properties is a major challenge because, by definition, topological states do not have a local order parameter. While a generic solution to this challenge is not available yet, topological states that are protected by a symmetry can be identified by distinctive degeneracies in their entanglement spectrum. Here, we provide two complementary protocols to probe these degeneracies based on, respectively, symmetry-resolved entanglement entropies and measurement-based computational algorithms. The interchangeability of the two protocols illustrates a deep link between the topological classification of quantum phases of matter and the computational power of their ground states. Both protocols are implemented on an IBM quantum computer and used to identify the topological cluster state. The comparison between the experimental findings and noisy simulations allows us to study the stability of topological states to perturbations and noise.

One of the most important achievements in modern physics is the discovery and classification of topological phases of matter. Topological states do not break any local symmetry and, hence, are robust against local perturbations. In the context of quantum computation, this protection can be used to perform quantum protocols that are robust to local noise sources. The downside of this protection is that local probes are insufficient to identify topological states. Hence, even if one is able to create a topological state, demonstrating its topological character can be very challenging. In this work, we take advantage of the exquisite tunability of superconducting circuits to both realize and identify a family of symmetry-protected topological (SPT) states.

SPT phases can be identified by inspecting their entanglement spectrum (ES), i.e., the set of eigenvalues of the reduced density matrix of a subsystem, ρ_A . In particular, for ground states of one dimensional (1D) SPT phases the ES is always formed by degenerate pairs (or multiplets), while in topologically trivial states there is no protected degeneracy [1, 2] [64]. This observation stands at the basis of the classification of all SPT phases in one and higher dimensions [3]. A simple explanation for the existence of ES degeneracies is offered by the symmetry-resolved structure of ρ_A [4, 5]. Consider a SPT phase protected by a unitary symmetry $G = G_A \times G_B$, where G_A and G_B act on subsystems A and B , respectively. Because G commutes with the Hamiltonian, the ground state of the SPT phase, $|\psi_{\text{gs}}\rangle$, is an eigenstate of the symmetry operator G . When performing a partial trace $\rho_A = \text{Tr}_B[|\psi_{\text{gs}}\rangle\langle\psi_{\text{gs}}|]$, the conservation of G guarantees that ρ_A is block diagonal in G_A , see Fig. 1. One can then define symmetry-resolved reduced density matrices as $\tilde{\rho}_A = \Pi_A \rho_A \Pi_A$, where Π_A projects a state on a specific symmetry sector. For simple SPTs, like the Haldane phase of integer spins or Kitaev chains, it was found [6, 7] that $\tilde{\rho}_A$ that belong to different sectors are identical, leading to a degenerate ES [65].

A related property of SPT phases is the possibility to use their ground states as resources for measurement-based quantum computation (MBQC), where the process of computation is driven by local measurements. This connection was uncovered in Ref. [8] for a measurement-based-adiabatic hybrid. Also, Ref. [9] described a method for realizing 1-qubit unitary logical gates with (non-unit) fidelity above 1/4 in a 1D SPT phase. Ref. [10] established that the quantum-wire-protocol is a uniform property of all ground states belonging to a given SPT phase of 1D spin chains. This result was subsequently extended to include measurement-based quantum gates in 1D SPT phases [11, 12] and finally to universal MBQC in 2D SPT

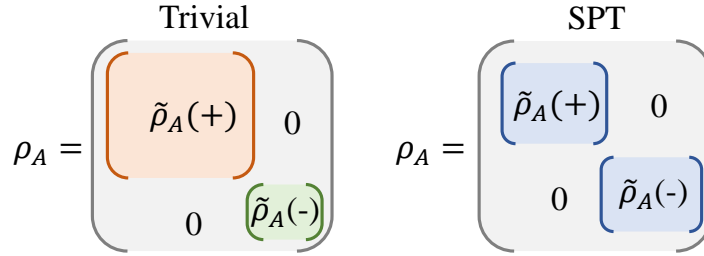


FIG. 1: Schematic distinction between trivial states and symmetry-protected-topological ones. In both cases the ground state commutes with the symmetry and the reduced density matrix ρ_A is block diagonal. In the topological states all blocks are identical, $\tilde{\rho}_A(+)$ = $\tilde{\rho}_A(-)$ in this example, while in the trivial state they are generically different.

phases [13–16].

Here, we use symmetry-resolved density matrices and MBQC protocols to identify the SPT properties of a quantum state. First, we implement a quantum protocol that accesses each symmetry sector individually. The equivalence of the different sectors helps us identify SPT states and distinguish them from trivial ones. Next, we implement the simplest protocol of quantum information processing in SPT states, namely the quantum wire protocol [10], and experimentally demonstrate its robustness under symmetry-respecting perturbations. The protocol can be disturbed only by perturbations that break the symmetry and make the state trivial, hence providing a complementary method to identify SPT states.

I. CLUSTER STATE

Having in mind the physical realization of our algorithm using qubits, we focus here on the 1D cluster Ising Hamiltonian

$$H_{\text{cluster}} = - \sum_i h_i = - \sum_i Z_{i-1} X_i Z_{i+1}, \quad (1)$$

where $\{X, Y, Z\}$ are Pauli matrices and h_i are referred to as stabilizers [9, 17–28]. Its ground state, also known as the 1D cluster state $|\psi_{\text{cluster}}\rangle$, is a topological state protected by the $Z_2 \times Z_2$ symmetry associated with the conservation of $P_{\text{odd}} = \prod_i h_{2i+1} = \prod_i X_{2i+1}$ and $P_{\text{even}} = \prod_i h_{2i} = \prod_i X_{2i}$. These operators correspond to parities on the sublattices of odd and even sites, respectively. For periodic boundary conditions, the reduced density matrix ρ_A

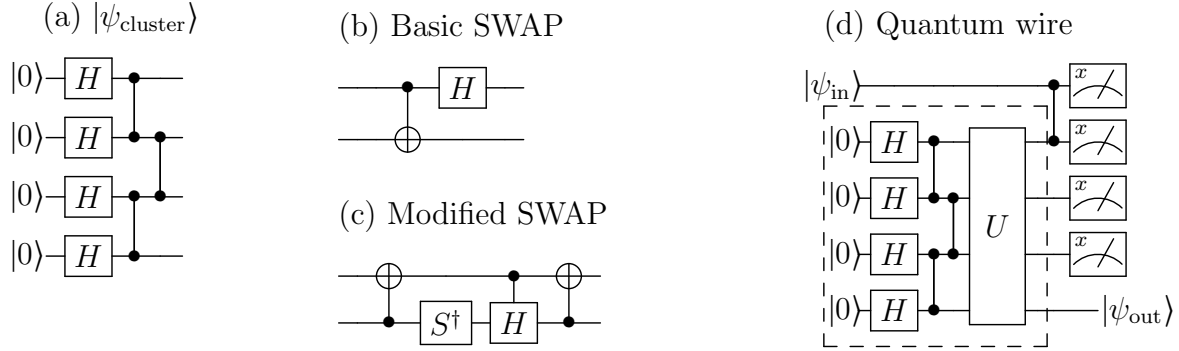


FIG. 2: Building blocks of the quantum circuits used in this article: (a) Preparation of the cluster state $|\psi_{\text{cluster}}\rangle$. (b) Basic SWAP test, which takes the singlet to $|11\rangle$, and the triplets to a mixture of $|00\rangle, |01\rangle, |10\rangle$, reproduced from Ref. [31, 32]. (c) Modified SWAP test, which identifies all four eigenvectors of $(Z_i \otimes I)\text{SWAP}$. This gate is used to compute symmetry-resolved purities. (d) Measurement-based quantum teleportation algorithm, using the state $U|\psi_{\text{cluster}}\rangle$ as a resource. See also Appendix VI B for the full quantum circuits.

of the cluster state has 4 identical eigenvalues $\lambda = 1/4$, one for each sector of the $Z_2 \times Z_2$ symmetry, see Appendix A.

The Hamiltonian H_{cluster} can be obtained from a trivial Hamiltonian $H_{\text{trivial}} = -\sum_i X_i$ by the transformation $X_i \rightarrow Z_{i-1}X_iZ_{i+1}$ and $Z_i \rightarrow X_i$. [66] This transformation can be used to prepare the cluster state in a quantum computer [29, 30]: Starting from the $|000\dots\rangle$ state, one needs to, first, apply Hadamard gates to bring the system to the ground state of H_{trivial} , $|\psi_{\text{trivial}}\rangle = |++++\dots\rangle$ and, then, apply controlled-Z gates on neighboring sites to perform the aforementioned unitary transformation, see Fig. 2(a) [67]. If the last qubit is not linked to the first one, see Fig. 2(a), one obtains a system with open boundary conditions. In this case, the first and last terms of the corresponding Hamiltonian, see Eq. (1), become $h_1 = X_1Z_2$ and $h_L = Z_{L-1}X_L$ and the state conserves the total parity $P = -\prod_{i=1}^L h_i = Y_1X_2X_3\dots X_{L-1}Y_L$.

II. SYMMETRY-RESOLVED ENTROPIES

As mentioned in the introduction, we use symmetry-resolved reduced density matrices, $\tilde{\rho}_A$, to identify the SPT nature of the cluster state. A direct measure of these matrices requires an exponentially large number of measurements. We overcome this difficulty by addressing the moments of these matrices, $\tilde{S}_n = \text{Tr}[\tilde{\rho}_A^n]$, which can be measured by realizing n copies of the state [33–42]. Specifically, for $n = 2$, this approach is based on the identity

$$\text{Tr}[\rho^2] = \text{Tr}[\rho_2 \text{ SWAP}]. \quad (2)$$

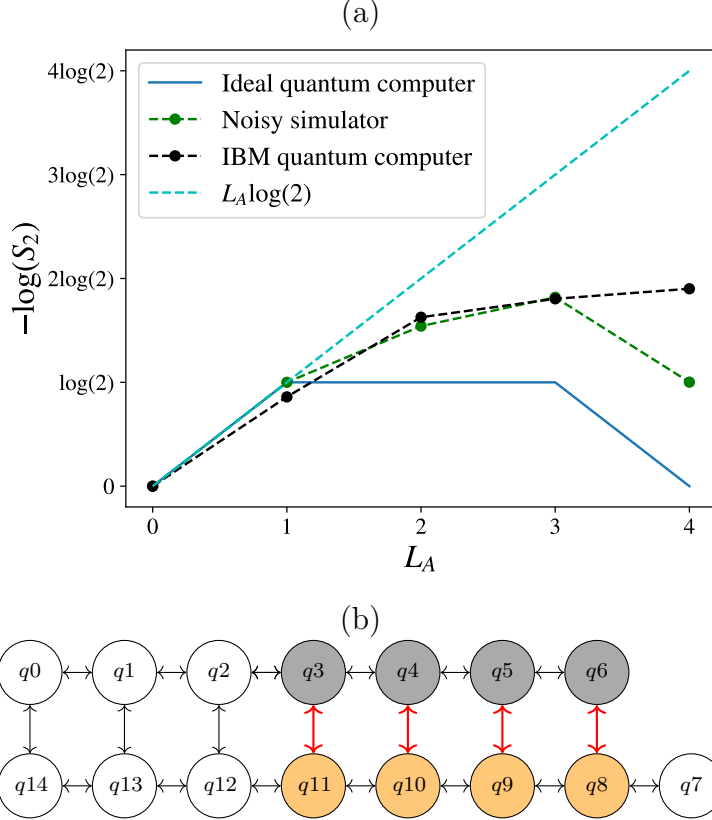


FIG. 3: Realization and characterization of a cluster state $|\psi_{\text{cluster}}\rangle$ with $L = 4$ qubits. (a) Second Rényi entropy as a function of the subsystem size L_A . (b) Connectivity of the Melbourne IBM quantum processor: The two copies of the cluster states were realized on gray and orange qubits, respectively; The two-qubit gates in red were used to realize SWAP operations between pairs of qubits on the two copies.

Here $\rho_2 = \rho \otimes \rho$ is the combined state of two independently prepared copies of a state, and the operator SWAP swaps arbitrary states of the two copies. By applying the SWAP operator only to the subsystem A , one can compute the purity of A , $\text{Tr}[\rho_A^2]$. Finally, if the SWAP operator is measured along with the projector to the conserved sectors, one can directly obtain the symmetry-resolved entropy \tilde{S}_n [37, 43, 44] [68].

To implement these ideas on a quantum computer, we create two copies of the cluster state with $L = 4$ qubits using two copies of the circuit of Fig. 2(a). Next, we measure the SWAP operator on each pair of qubits of the two copies, using 4 copies of the quantum circuit introduced by Refs. [31, 32], see Fig. 2(b) [69]. By repeatedly measuring the output of the circuit, we infer the expectation values of the products of the SWAP operators of each site of a subsystem A , which correspond to $S_2 = \text{Tr}[\rho_A^2]$. In Fig. 3(a) we plot $-\log S_2$, also known as the *second Rényi entropy*, as a function of the subsystem size L_A . The result

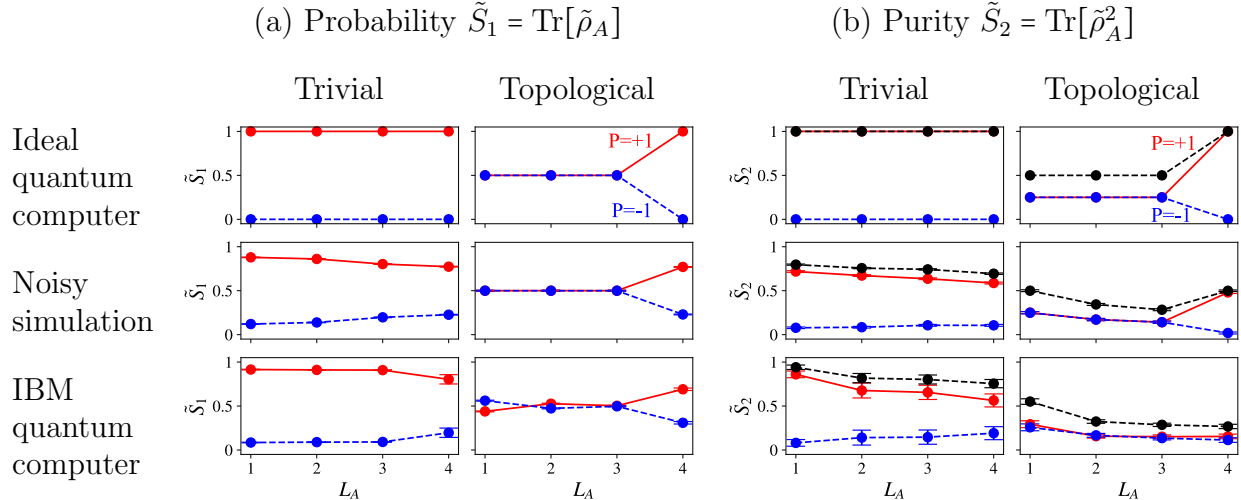


FIG. 4: Symmetry-resolved entanglement measures \tilde{S}_1 and \tilde{S}_2 , for the trivial state $|\psi_{\text{trivial}}\rangle$ and for the topological state $|\psi_{\text{cluster}}\rangle$. The even parity $P = +1$, odd parity $P = -1$, and total contributions are shown in blue, red and black, respectively.

of this calculation matches the known properties of the cluster state with open boundary conditions: For any $0 < L_A < L$, ρ_A has 2 identical eigenvalues $\lambda = 1/2$, one for each sector of the symmetry P , and one has $S_2 = 1/2$. Importantly, for $L_A = L$ one has $S_2 = \text{Tr}[\rho^2] = 1$, indicating that the system is pure.

We now turn to symmetry-resolved measurements, which can unveil the SPT nature of a state. The first moment, $\tilde{S}_1 = \text{Tr}[\tilde{\rho}_A]$, is simply the probability to find a subsystem in a specific sector of the symmetry. To compute the second moment, we design a circuit that measures the value of the SWAP and P operators at the same time, see Fig. 2(c) and Methods section. The results of these calculations are shown in the upper panel of Fig. 4: For the trivial state, the entire weight lies in the even parity sector, $P = +1$. For the cluster state, the full system ($L_A = L$) is still an eigenvector of P with $P = +1$. In contrast, smaller subsystems ($L_A < L$) occupy with equal probabilities the sectors $P = +1$ and $P = -1$, in agreement with the topologically-protected degeneracy of the two symmetry-resolved reduced density matrices.

III. NOISY SPT STATES

To understand actual experiments with superconducting circuits, it is necessary to study the effect of noise on topological states. Several earlier works addressed this question by

extending the topological classification of pure states to density matrices [45–53]. Here, we focus on the effect of noise on the degeneracies of the ES, as probed by symmetry-resolved reduced density matrices. We then define a noise source to be symmetry preserving if it preserves this degeneracy (and vice versa), see the Methods section for a formal definition. Let us now consider the results of a noisy simulation, obtained using QISKIT AER (version 0.3.4) by IBM Research. The simulator computes the evolution of the density matrix by taking into account realistic noise sources in terms of Kraus operators. The parameters used in the simulation are determined by direct measurements of the success probability of the gates in the physical system [70]. Interestingly, all noise sources present in this simulation are symmetry preserving [54], with the exception of a measurement bias that leads to a systematic error towards 0 outcomes. To study the effects of symmetry preserving noise sources, we manually eliminate this bias from the simulations. In this case, if the system is prepared in an SPT state belonging to the same universality class as the cluster state, the noise does not lift the ES degeneracies.

We first consider the effects of noise on $S_2 = \text{Tr}[\rho^2]$, see Fig. 3(a). In the presence of noise, the state is not pure and the second Rényi entropy of the full system is $\approx 1.1 \times \log(2)$. This value is significantly smaller than the maximally allowed value of $4 \times \log(2)$, indicating that the output of the simulation is not trivial. The slope of the entropy changes in the second half of the chain, as in the ideal quantum computer. To study the SPT properties of this noisy state, we compute symmetry-resolved quantities, see Fig. 4. For the trivial state, we find that both the probability and the symmetry-resolved purity are larger for $P = +1$ than for $P = -1$. In contrast, in the cluster state the probabilities and purities are identical for the two sectors for all $L_A < L$. Remarkably, the total system ($L_A = L$) is mostly found in the $P = +1$ state, confirming that the system is targeting the correct pure state.

Using the same QISKIT package, we performed the same calculations on the 15-qubit Melbourne IBM quantum computer (ibmq_16_melbourne) on December 26-28, 2019, using 150 runs with 8192 measurements each. This computer has 15 qubits organized in a ladder structure, with physical two-qubit gates between nearest neighbors only. This structure is ideal for the circuit under the present consideration: we realize the two copies of the cluster states on the two parallel chains that form the ladder, and use the rungs to realize the SWAP operators, see Fig. 3(b). The results obtained in the actual computer are similar to those observed in the simulator: although the purity of the cluster state is not

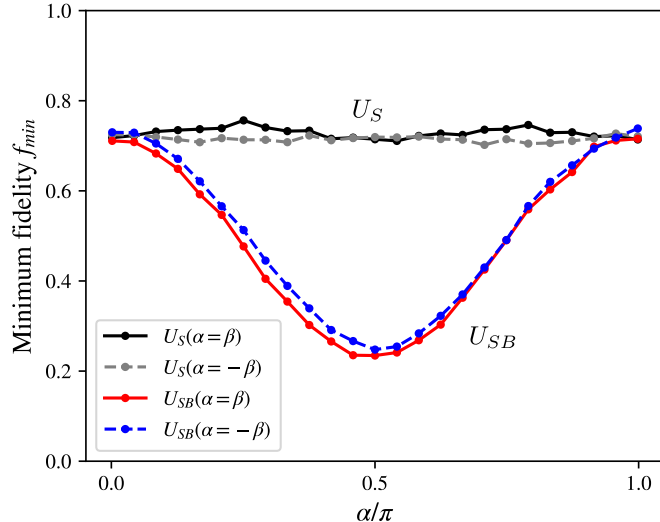


FIG. 5: Fidelity of the measurement-based teleportation algorithm under the influence of symmetry-(non)preserving perturbations. Each data point represents the minimal fidelity with respect to 6 initial states (see SI VIC for the raw data).

ideal, our symmetry resolved probes still correctly identify its SPT nature. One interesting difference between the quantum computer and the noisy simulator can be observed in the symmetry resolved probes of small subsystems, $L_A = 1, 2$. In the actual computer, the two sectors show small, but statistically significant, differences. We identify these errors as due to symmetry-breaking noise sources, such as the aforementioned measurement bias, which were absent in the simulation but present in the physical system. This bias also explains why the Rényi entropy of the $L_A = 1$ subsystem (Fig. 3(a)) is smaller than $1/2$, see Methods section. Our results demonstrate that topological arguments can be used to characterize the main sources of errors and classify them according to their symmetry.

IV. MEASUREMENT-BASED WIRE PROTOCOL

We now turn to the experimental realization of the symmetry-protected wire protocol [10]. In this protocol, a general quantum state is encoded in one boundary of the spin chain. The state is, then, shuttled to the other boundary in a teleportation-like fashion, by local measurements of the spins along the chain. We apply this protocol to a family of SPT states with $\mathbb{Z}_2 \times \mathbb{Z}_2$ symmetry, which contains the 1D cluster state as a special case. All states in the family possess the same SPT order and, hence, have the same capacity to transmit

one-qubit-worth of quantum information. Our goal is to verify the robustness of the protocol against variation within the phase.

For our implementation on an IBM quantum computer we use the $L = 4$ cluster state $|\psi_{\text{cluster}}\rangle$ described above. The corresponding $\mathbb{Z}_2 \times \mathbb{Z}_2$ symmetry is generated by $P_{\text{odd}} = \prod_{i=1,3} h_i = X_1 X_3 Z_4$ and $P_{\text{even}} = \prod_{i=2,4} h_i = Z_1 X_2 X_4$, where h_i are defined in Eq. 1. The family of SPT states is created applying either symmetry-preserving unitaries $U_S(\alpha, \beta) = e^{i\beta Z_1 X_2 Z_3} e^{i\alpha X_3}$, or symmetry-breaking unitaries $U_{SB}(\alpha, \beta) = e^{i\beta Z_1 X_2 Z_3} e^{i\alpha Y_3}$ to $|\psi_{\text{cluster}}\rangle$. In the former case all resource states respect the $\mathbb{Z}_2 \times \mathbb{Z}_2$ symmetry and can be continuously connected in a symmetry-respecting fashion to the cluster state. In the latter case, the symmetry is broken and computational uniformity is not guaranteed.

Next, we introduce another qubit realizing the input state $|\psi_{in}\rangle$ and teleport it into the wire by performing a measurement in the 2-qubit cluster basis (a locally rotated Bell basis, $\{|+0\rangle \pm |-1\rangle\}$) on $|\psi_{in}\rangle$ and the first qubit of the spin chain, see Fig. 2(d). This particular measurement is chosen to be compatible with the MBQC wire protocol, consisting of local measurements in the X-basis of the remaining qubits, and classically controlled Pauli correction depending on the measurement outcomes. Fig. 5 shows the experimentally measured minimum fidelity $f_{\min} = \min_i \langle \psi_{in}^i | \rho_{out}^{exp} | \psi_{in}^i \rangle$ for six different input states $|\psi_{in}^i\rangle$ and the Pauli-corrected output state ρ_{out}^{exp} resulting from the wire protocol, for the choices $\beta = \pm\alpha$ in both the symmetric and the symmetry-breaking case, see also Appendix VI C. We find that the transmission fidelity is constant as a function of α in the symmetry-respecting case. In the symmetry-breaking case, the transmission fidelity is non-constant as the resource state is varied.

V. CONCLUSION

In this paper we proposed and realized experimentally two algorithms to identify the SPT nature of the cluster state on a quantum computer. The first algorithm stems from the observation that in SPT states, the reduced density matrix ρ_A is formed by identical blocks that correspond to different sectors of the underlying symmetry. The flexibility of the quantum computer allowed us to directly probe the moments of density matrices by projecting the quantum state into the different symmetry sectors. The realization of this algorithm on both a quantum simulator and on a IBM quantum computer allowed us to study the impact

of time dependent noise on the SPT order of the state. In particular, we found that while most of realistic noise sources are symmetry preserving, the systematic measurement bias of the physical machine breaks this symmetry. Its effects are, however, small enough to enable us to identify the SPT nature of the cluster state. An alternative way to characterize the SPT order of the cluster states consists of using them as a buffer for measurement based quantum teleportation. We find that the fidelity of this protocol is unaffected by symmetry preserving terms, and vice versa for symmetry breaking terms.

Our work has important implications for the modelling of noisy intermediate-scale quantum computers. We have demonstrated that topological arguments are an efficient tool to identify and classify noise sources in quantum computers. This information can be used to improve the performance of quantum computers, for example, by gauging the measurement apparatus to take into account systematic errors. From a fundamental perspective, we identified sufficient conditions under which a noisy quantum state can retain its SPT properties. This aspect may have implications for quantum computations: for pure states, it was shown that the classification of SPT phases is in one-to-one correspondence with the possibility to use it as a resource for one-way-quantum computer. Although this question deserves further investigation, we conjecture that this link extends to noisy systems as well.

VI. METHODS

1. Quantum algorithm to compute the symmetry resolved purity – The symmetry resolved purity of the subsystem A of size $L_A < L$ is defined by $\tilde{S}_2(P) = \text{Tr}[\rho_A^2 \Pi_A(P)]$, where $\Pi_A(\pm 1) = (1 \pm Y_1 X_2 \dots X_{L_A})/2$ is the projection over the $P = \pm 1$. We implement this circuit by taking the average between the expectation values of $\text{Tr}[\rho_A^2]$ and $\text{Tr}[\rho_A^2 Y_1 X_2 \dots X_{L_A}]$. To compute the latter, we implement two copies of the same state, according to Eq. (1). For simplicity, let us focus on a single qubit i , where the operator $\text{Tr}[\rho_A^2 X_i]$ can be written as $\text{Tr}[\rho_2(X_i \otimes I) \text{SWAP}_i]$ and SWAP_i swaps the two copies of the qubit i . The operator $O_i = (X_i \otimes I) \text{SWAP}_i$ is unitary, $O_i^\dagger O_i = 1$ with eigenvectors $\{|++\rangle, |--\rangle, \frac{|+-\rangle + |-+\rangle}{\sqrt{2}}, \frac{|+-\rangle - |-+\rangle}{\sqrt{2}}\}$ and eigenvalues $\{\lambda_i\} = \{1, -1, i, -i\}$. This local basis change is performed in Fig. 1(c) using the Z basis and needs to be rotated to the X basis for $i > 2$ (or the Y basis for $i = 1$). To obtain $\text{Tr}[\rho_A^2 \Pi_A]$, after performing a measurement on each pair of copies and classically recording the appropriate eigenvalue λ_i , we perform a quantum average over $\prod_{i=1}^{L_A} \lambda_i$. This method generalizes for any moment n and for general symmetry (such as Z_N), hence generalizing the symmetry-resolved entanglement protocols of Refs. [6, 37] to qubits.

2. Formal definition of symmetry preserving noise sources – A formal definition of symmetry preserving noise sources can be given by introducing an operator T_A , which acts on a subsystem A and maps the different sectors of the symmetry among themselves. In a SPT

state, all symmetry-resolved reduced density matrices are identical and hence $[T_A, \rho_A] = 0$. In the example of the cluster state the operators T_A flip the edge spins X_1 and X_{L_A} and are given by Z_1 and Z_{L_A} . A generic noise map $\Phi : \rho_A \rightarrow \rho'_A$ is then said to be symmetry-preserving if it preserves the property $[T_A, \rho'_A] = 0$. Specifically, we focus on noise sources that can be described by the Kraus operators according to

$$\Phi : \rho \rightarrow \rho' = \sum_i K_i \rho K_i^\dagger \quad (3)$$

with the normalization condition $\sum_i K_i^\dagger K_i = I$, where I is the identity matrix. A trivial example of a symmetry-preserving noise is dephasing, described by the Kraus operators $K_1 = \sqrt{1-p}I$ and $K_2 = \sqrt{p}Z_i$. Both operators conserve Z_i and commute with T_A . A non-trivial example is given by the depolarizing noise with $K_1 = [(1+\sqrt{1-p})I - (1-\sqrt{1-p})Z_i]/2$ and $K_2 = \sqrt{p}\sigma_i^-$. These operators do not conserve Z and, hence, do not commute with T_A . However, because σ_i^- commutes with the product of two K_i , if $[\rho, Z_i] = 0$ then $[\rho', Z_i] = 0$ leading to symmetry preservation. These examples highlight the difference between conserved quantities and symmetries: a conserved quantity is always a symmetry, but not vice versa (see Refs. [55–57] for an introduction).

3. A simple model of the measurement bias – A natural candidate for the symmetry-breaking noise observed in the quantum computer is a systematic error present in the measurement device, giving preference to state 0 with respect to state 1, or vice versa. The existence of this error explains why the second Rényi entropy $-\log[S_2]$ at $L_A = 1$ is smaller than $\log 2$, see Fig. 3(a): If we assume that the output qubits are random variables with probabilities $0.5 \pm \epsilon$, we obtain $-\log S_2 = -L_A \log[(0.5 + \epsilon)^2 + (0.5 - \epsilon)^2] \approx L_A(\log 2 - 4\epsilon^2)$. In the same model, the difference between the even and odd probabilities decreases exponentially as $|\tilde{S}_n(P = +1) - \tilde{S}_n(P = -1)| = |(0.5 + \epsilon)^n - (0.5 - \epsilon)^n| \approx |2^{2-n} n \epsilon|^{L_A}$. These expressions are in qualitative agreement with the experimental observations for $|\epsilon| \approx 2\%$, see Figs. 3 and 4.

Acknowledgments We acknowledge useful discussions with Yael Ben-Haim, Moshe Goldstein, Joe Jackson, Yuval Tamir, Ari Turner, Hannes Pichler, Frank Pollmann. We acknowledge support from ARO (W911NF-20-1-0013) (RR and ES). This work is supported by the Israel Science Foundation, grants number 151/19 (DA and EGDT), 154/19 (DA, YN, ES and EGDT).

Competing Interests The authors declare that there are no competing interests.

Author Contribution – D.A. and R.H. performed the experimental measurements of, respectively, the symmetry-resolved entropies and the measurement-based wire protocol. Y.N., R.R., E.S. and E.G.D.T. supervised the project. All authors contributed to the theoretical ideas developed in this article and to the writing of the manuscript.

Data Availability All QISKIT Python codes used in this paper, as well as the raw exper-

imental results, are available from the corresponding author upon request.

-
- [1] Pollmann, F., Turner, A. M., Berg, E., and Oshikawa, M. *Physical Review B* **81**(6), 064439 (2010).
 - [2] Fidkowski, L. *Physical Review Letters* **104**(13), 130502 (2010).
 - [3] Chen, X., Gu, Z.-C., Liu, Z.-X., and Wen, X.-G. *Physical Review B* **87**(15), 155114 (2013).
 - [4] Laflorencie, N. and Rachel, S. *Journal of Statistical Mechanics: Theory and Experiment* **2014**(11), P11013 (2014).
 - [5] Goldstein, M. and Sela, E. *Physical Review Letters* **120**(20), 200602 (2018).
 - [6] Cornfeld, E., Landau, L. A., Shtengel, K., and Sela, E. *Physical Review B* **99**(11), 115429 (2019).
 - [7] Fraenkel, S. and Goldstein, M. *arXiv preprint arXiv:1910.08459* (2019).
 - [8] Miyake, A. *Physical Review Letters* **105**(4), 040501 (2010).
 - [9] Doherty, A. C. and Bartlett, S. D. *Physical Review Letters* **103**(2), 020506 (2009).
 - [10] Else, D. V., Schwarz, I., Bartlett, S. D., and Doherty, A. C. *Physical Review Letters* **108**(24), 240505 (2012).
 - [11] Miller, J. and Miyake, A. *Physical Review Letters* **114**(12), 120506 (2015).
 - [12] Raussendorf, R., Wang, D.-S., Prakash, A., Wei, T.-C., and Stephen, D. T. *Physical Review A* **96**(1), 012302 (2017).
 - [13] Raussendorf, R., Okay, C., Wang, D.-S., Stephen, D. T., and Nautrup, H. P. *Physical Review Letters* **122**(9), 090501 (2019).
 - [14] Devakul, T. and Williamson, D. J. *Physical Review A* **98**(2), 022332 (2018).
 - [15] Stephen, D. T., Nautrup, H. P., Bermejo-Vega, J., Eisert, J., and Raussendorf, R. *Quantum* **3**, 142 (2019).
 - [16] Daniel, A. K., Alexander, R. N., and Miyake, A. *arXiv preprint arXiv:1907.13279* (2019).
 - [17] Gottesman, D. *arXiv preprint quant-ph/9705052* (1997).
 - [18] Briegel, H. J. and Raussendorf, R. *Physical Review Letters* **86**(5), 910 (2001).
 - [19] Keating, J. and Mezzadri, F. *Communications in mathematical physics* **252**(1), 543–579 (2004).
 - [20] Kopp, A. and Chakravarty, S. *Nature Physics* **1**(1), 53–56 (2005).
 - [21] Son, W., Amico, L., Fazio, R., Hamma, A., Pascazio, S., and Vedral, V. *EPL (Europhysics Letters)* **95**(5), 50001 (2011).
 - [22] Smacchia, P., Amico, L., Facchi, P., Fazio, R., Florio, G., Pascazio, S., and Vedral, V. *Physical Review A* **84**(2), 022304 (2011).
 - [23] Niu, Y., Chung, S. B., Hsu, C.-H., Mandal, I., Raghu, S., and Chakravarty, S. *Physical Review B* **85**(3), 035110 (2012).
 - [24] DeGottardi, W., Thakurathi, M., Vishveshwara, S., and Sen, D. *Physical Review B* **88**(16), 165111 (2013).
 - [25] Lahtinen, V. and Ardonne, E. *Physical Review Letters* **115**(23), 237203 (2015).
 - [26] Ohta, T., Tanaka, S., Danshita, I., and Totsuka, K. *Physical Review B* **93**(16), 165423 (2016).
 - [27] Lee, T. E., Joglekar, Y. N., and Richerme, P. *Physical Review A* **94**(2), 023610 (2016).
 - [28] Friedman, B.-E., Rajak, A., and Dalla Torre, E. G. *EPL (Europhysics Letters)* **125**(1), 10008 (2019).
 - [29] Choo, K., von Keyserlingk, C. W., Regnault, N., and Neupert, T. *Physical Review Letters*

- 121**, 086808 Aug (2018).
- [30] Smith, A., Jobst, B., Green, A. G., and Pollmann, F. *arXiv preprint arXiv:1910.05351* (2019).
 - [31] Garcia-Escartin, J. C. and Chamorro-Posada, P. *Physical Review A* **87**(5), 052330 (2013).
 - [32] Cincio, L., Subaşı, Y., Sornborger, A. T., and Coles, P. J. *New Journal of Physics* **20**(11), 113022 (2018).
 - [33] Daley, A. J., Pichler, H., Schachenmayer, J., and Zoller, P. *Physical Review Letters* **109**(2), 020505 (2012).
 - [34] Pichler, H., Bonnes, L., Daley, A. J., Läuchli, A. M., and Zoller, P. *New Journal of Physics* **15**(6), 063003 (2013).
 - [35] Islam, R., Ma, R., Preiss, P. M., Tai, M. E., Lukin, A., Rispoli, M., and Greiner, M. *Nature* **528**(7580), 77 (2015).
 - [36] Johri, S., Steiger, D. S., and Troyer, M. *Physical Review B* **96**(19), 195136 (2017).
 - [37] Cornfeld, E., Goldstein, M., and Sela, E. *Physical Review A* **98**(3), 032302 (2018).
 - [38] Cornfeld, E., Sela, E., and Goldstein, M. *Physical Review A* **99**(6), 062309 (2019).
 - [39] Bonsignori, R., Ruggiero, P., and Calabrese, P. *Journal of Physics A: Mathematical and Theoretical* **52**(47), 475302 (2019).
 - [40] Feldman, N. and Goldstein, M. *Physical Review B* **100**(23), 235146 (2019).
 - [41] Murciano, S., Di Giulio, G., and Calabrese, P. *arXiv preprint arXiv:1911.09588* (2019).
 - [42] Tan, M. T. and Ryu, S. *arXiv preprint arXiv:1911.01451* (2019).
 - [43] Xavier, J., Alcaraz, F. C., and Sierra, G. *Physical Review B* **98**(4), 041106 (2018).
 - [44] Barghathi, H., Casiano-Diaz, E., and Del Maestro, A. *Physical Review A* **100**(2), 022324 (2019).
 - [45] Diehl, S., Rico, E., Baranov, M. A., and Zoller, P. *Nature Physics* **7**(12), 971 (2011).
 - [46] Viyuela, O., Rivas, A., and Martin-Delgado, M. *Physical Review Letters* **112**(13), 130401 (2014).
 - [47] van Nieuwenburg, E. P. and Huber, S. D. *Physical Review B* **90**(7), 075141 (2014).
 - [48] Andersson, O., Bengtsson, I., Ericsson, M., and Sjöqvist, E. *Philosophical Transactions of the Royal Society A: Mathematical, Physical and Engineering Sciences* **374**(2068), 20150231 (2016).
 - [49] Linzner, D., Wawer, L., Grusdt, F., and Fleischhauer, M. *Physical Review B* **94**(20), 201105 (2016).
 - [50] Gong, Z., Ashida, Y., Kawabata, K., Takasan, K., Higashikawa, S., and Ueda, M. *Physical Review X* **8**(3), 031079 (2018).
 - [51] Bardyn, C.-E., Wawer, L., Altland, A., Fleischhauer, M., and Diehl, S. *Physical Review X* **8**(1), 011035 (2018).
 - [52] Goldstein, M. *arXiv preprint arXiv:1810.12050* (2018).
 - [53] Asorey, M., Facchi, P., and Marmo, G. *arXiv preprint arXiv:1905.05539* (2019).
 - [54] https://github.com/Qiskit/qiskit-aer/blob/d8d77270c745e4c31129ce7f816a93e1efc2e743/qiskit/providers/aer/noise/errors/standard_errors.py. Accessed: 2019-11-21.
 - [55] Baumgartner, B. and Narnhofer, H. *Journal of Physics A: Mathematical and Theoretical* **41**(39), 395303 (2008).
 - [56] Albert, V. V. and Jiang, L. *Physical Review A* **89**(2), 022118 (2014).
 - [57] Buča, B. and Prosen, T. *New Journal of Physics* **14**(7), 073007 (2012).
 - [58] D. Azses, E. G. Dalla Torre, E. Sela, In preparation.
 - [59] Lindner, N. H. and Rudolph, T. *Physical Review Letters* **103**(11), 113602 (2009).
 - [60] Economou, S. E., Lindner, N., and Rudolph, T. *Physical Review Letters* **105**(9), 093601

- (2010).
- [61] Schwartz, I., Cogan, D., Schmidgall, E. R., Don, Y., Gantz, L., Kenneth, O., Lindner, N. H., and Gershoni, D. *Science* **354**(6311), 434–437 (2016).
 - [62] Buterakos, D., Barnes, E., and Economou, S. E. *Physical Review X* **7**(4), 041023 (2017).
 - [63] Pichler, H., Choi, S., Zoller, P., and Lukin, M. D. *Proceedings of the National Academy of Sciences* **114**(43), 11362–11367 (2017).
 - [64] The degeneracy of the ES of an SPT state is exact only in the thermodynamic limit where both the system size and the size of the subsystem tend to infinity. For finite size systems, the degeneracy is exponentially suppressed as the ratio between the (sub)system size and the correlation length of the state.
 - [65] A general relationship between symmetry sectors $\tilde{\rho}_A$ in arbitrary SPTs can be derived using cohomology theory [58].
 - [66] Incidentally, we note that by applying a similar transformation $X_i \rightarrow Z_{i-1}X_iZ_{i+1}$ and $Y_i \rightarrow Z_i$ multiple times, one obtains a series of topological states of increasing complexity [28, 58].
 - [67] See also related realizations using entangled photons [59–63]
 - [68] Mathematically, a proof of the equivalence between the symmetry sectors requires to access the full ES, demanding a number of measurements that grows with the size of the Hilbert space. However, in practice, it is often sufficient to check that the symmetry exists in the first few moments to demonstrate the SPT nature of the state.
 - [69] All circuits used in this paper can be found in Appendix VI B
 - [70] We used the noise model that matches the experiments’ date.

Supplementary Materials

A. Reduced density matrix of the cluster state

The properties of the cluster states can be derived by noting that all the stabilizers $h_i \equiv Z_{i-1}X_iZ_{i+1}$, commute among each other. Because h_i is Hermitian and squares to 1, its eigenvalues are ± 1 . For L qubits with periodic boundary conditions (and even L , in consistency with the $Z_2 \times Z_2$ symmetry), the 2^L common eigenvectors of the h_i ’s form an orthonormal basis. The ground state of the Hamiltonian H_{cluster} corresponds to the state satisfying $h_i|\psi_{\text{cluster}}\rangle = |\psi_{\text{cluster}}\rangle$ for all i .

We now use this construction to derive the reduced density matrix $\rho_A = \text{Tr}_B[|\psi_{\text{cluster}}\rangle\langle\psi_{\text{cluster}}|]$. Specifically, we consider as the subsystem A the qubits i with $1 \leq i \leq L_A$. The reduced density matrix is obtained from the Schmidt decomposition $|\psi_{\text{cluster}}\rangle = \sum_i \lambda_i |\psi_i^A\rangle |\psi_i^B\rangle$ as $\rho_A = \sum_i |\lambda_i|^2 |\psi_i^A\rangle\langle\psi_i^A|$. For a SPT phase it is convenient to perform the Schmidt decomposition in terms of edge states [1, 2]. Here, the left edge (ℓ) state of region A consists of Pauli operators $\mathcal{Z}_\ell = Z_1$ and $\mathcal{X}_\ell = X_1Z_2$ and for the right edge $\mathcal{Z}_r = Z_{L_A}$ and $\mathcal{X}_r = Z_{L_A-1}X_{L_A}$. It is sufficient to perform the Schmidt decomposition on the

subspace spanned by the few (four) stabilizers h_i that connect A and B across the two entanglement cuts. One finds that near each entanglement cut the joint stabilizer eigenstates are Bell states of the edge spins across each entanglement cut. Thus, in the basis $|\alpha = \pm 1\rangle$ ($|\beta = \pm 1\rangle$) of eigenstates of edge spins \mathcal{X}_ℓ (\mathcal{X}_r), we have $\rho_A = \frac{1}{4} \sum_{\alpha, \beta} |\alpha, \beta\rangle\langle\alpha, \beta|$. This expression indicates that ρ_A has 4 identical eigenvalues, $\lambda_i = 1/4$. Crucially, these edge operators represent the symmetry within the ground state. Using the fact that all stabilizers within the bulk of the subsystem satisfy $h_i = 1$, we have (for L_A odd and an obvious modification for L_A even) $P_{\text{odd}} = \mathcal{X}_\ell \mathcal{X}_r = \alpha\beta$ and $P_{\text{even}} = \mathcal{Z}_\ell \mathcal{Z}_r$. Diagonalizing the symmetries, we see that each eigenvalue belongs to a different sector of the symmetries $(P_{\text{even}}, P_{\text{odd}}) = (\pm 1, \pm 1)$. As expected for a SPT state, one obtains equal contributions from all symmetry sectors. For open-boundary conditions, there is only one edge in the Schmidt decomposition, resulting in $\rho_A = \frac{1}{2} \sum_\beta |\beta\rangle\langle\beta|$, which has 2 identical eigenvalues $\lambda_i = \frac{1}{2}$. Finally, for the topologically trivial state $|\psi_{\text{trivial}}\rangle$, which is a product state, the reduced density matrix has a single eigenvalue $\lambda = 1$ belonging to the sector $(P_{\text{even}}, P_{\text{odd}}) = (1, 1)$.

B. Quantum circuits used in this article

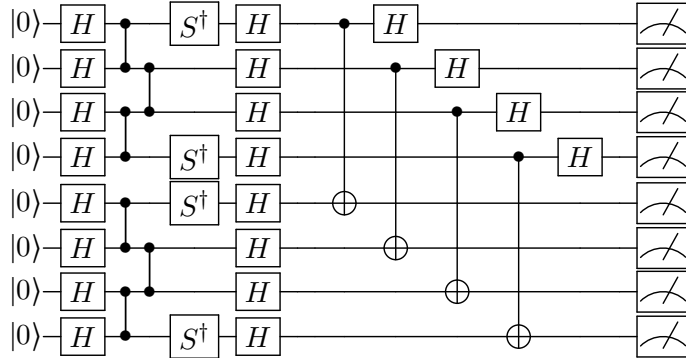


FIG. 6: Circuit for measuring the purity S_A .

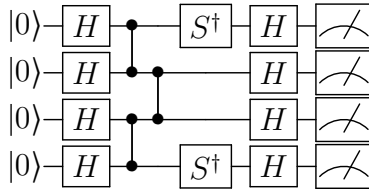


FIG. 7: Circuit for measuring the symmetry-resolved probabilities \tilde{S}_1^A .

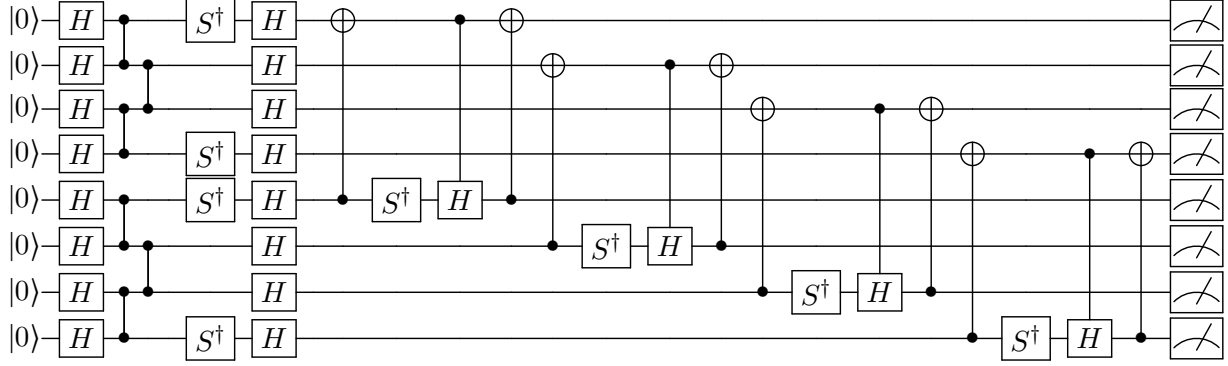


FIG. 8: Circuit for measuring the symmetry-resolved purities \tilde{S}_2^A .

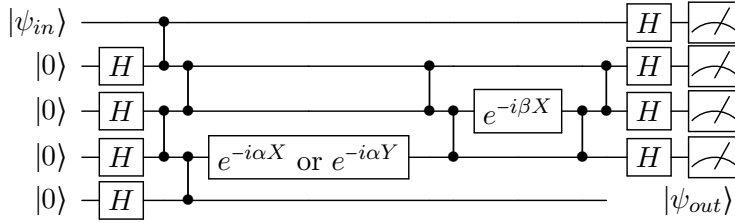


FIG. 9: Circuit for the measured-based teleportation algorithm with symmetry-preserving or symmetry-breaking perturbations.

C. Fidelity of the quantum teleportation algorithm

The fidelity of the quantum teleportation algorithm is defined as $F = |\langle \psi_{in} | \psi'_{out} \rangle|^2$, where $|\psi'_{out}\rangle = U |\psi_{out}\rangle$, $U = Z_{out}^{q_1} X_{out}^{q_2} Z_{out}^{q_3} X_{out}^{q_4}$, and $\{q_1, q_2, q_3, q_4\}$ are the measured values of the wire qubits in the x basis [10]. For a mixed output state characterized by the density matrix ρ_{out} , the fidelity generalizes to $F = \langle \psi_{in} | U \rho_{out} U^\dagger | \psi_{in} \rangle$. We measure ρ_{out} by full state tomography, i.e. by measuring the expectation values of X , Y and Z and using $\rho_{out} = (1 + \langle X_{out} \rangle \sigma^x + \langle Y_{out} \rangle \sigma^y + \langle Z_{out} \rangle \sigma^z) / 2$. The fidelity of the quantum teleportation algorithm is computed for 6 different initial states:

$$|0\rangle, |1\rangle, |+\rangle, |-\rangle, |\odot\rangle = \frac{1}{\sqrt{2}}(|0\rangle + i|1\rangle), |\ominus\rangle = \frac{1}{\sqrt{2}}(|0\rangle - i|1\rangle).$$

The results of our algorithm for each individual initial state are shown in Fig. 10. Each data point is obtained by averaging over 8192 measurements.

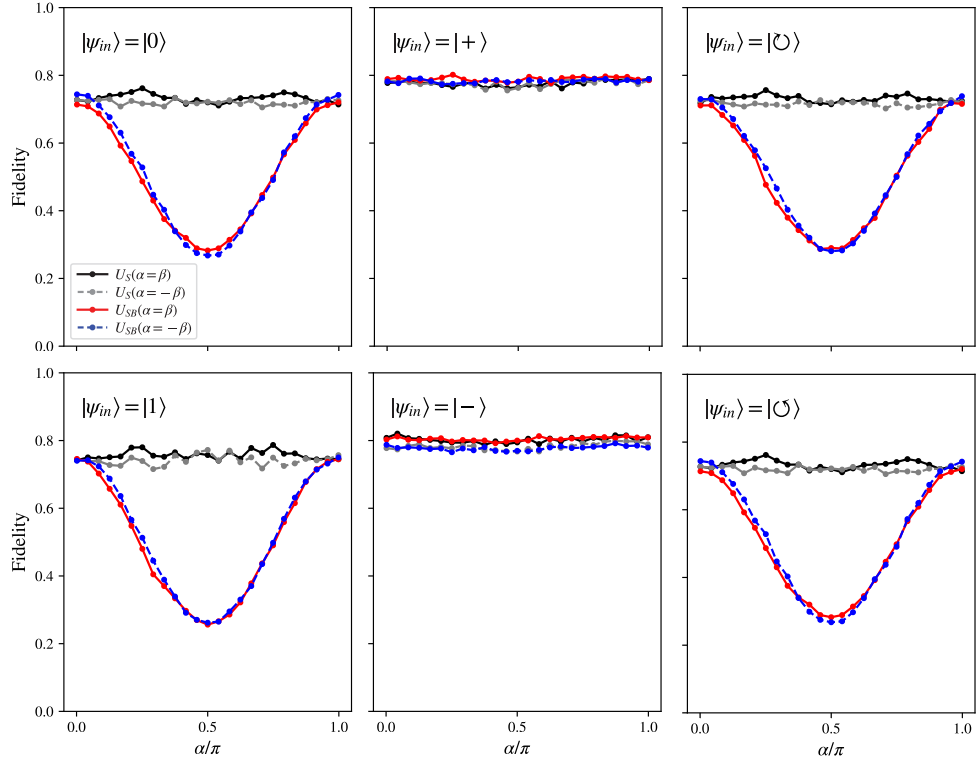


FIG. 10: Fidelity of the teleportation algorithm for six different initial states.